(4) E. von Jenckel, E. Teege, and W. Hinrichs, *Kolloid Z. Z. Polym.*, **129**, 19 (1952).
(5) H. Schonhorn, *J. Polym. Sci., Part B*, **2**, 465 (1964).
(6) P. R. Fitchmun and S. Newman, *J. Polym. Sci., Part A-2*, **8**, 1545 (1970).
(7) F. P. Price and R. W. Kilb, *J. Polym. Sci.*, **57**, 395 (1962).
(8) K. Sasaguri, R. Yamada, and R. S. Stein, *J. Appl. Phys.*, **35**, 3188 (1964).
(9) Y. Fujiwara, *Kolloid Z. Z. Polym.*, **226**, 135 (1968).
(10) J. M. Crissman and E. Passaglia, *J. Res. Natl. Bur. Stand., Sect. A*, **70**, 225 (1966).
(11) J. M. Crissman, *J. Polym. Sci., Part A-2*, **6**, 389 (1968).
(12) W. G. Pfann, "Zone Melting", 2nd ed, Wiley, New York, N.Y., 1966.
(13) M. Zief, "Fractional Solidification", M. Zief and W. R. Wilcox, Ed., Marcel Dekker, New York, N.Y., 1967, pp 649–678.
(14) F. W. Peaker and J. C. Robb, *Nature (London)*, **182**, 1591 (1956).
(15) J. D. Loconti and J. W. Cahill, *J. Polym. Sci.*, **49**, 52 (1961).
(16) A. M. Ruskin and G. Parravano, *J. Appl. Polym. Sci.*, **8**, 565 (1964).
(17) H. D. Keith and F. J. Padden, *J. Appl. Phys.*, **35**, 1270 (1964); **35**, 1286 (1964).
(18) A. Mehta and B. Wunderlich, *Colloid Polym. Sci.*, **253**, 193 (1975).
(19) H. D. Keith and F. J. Padden, *J. Appl. Phys.*, **34**, 2409 (1963).
(20) K. Tanaka, T. Seto, and Y. Fujiwara, *Rep. Prog. Polym. Phys. Jpn.*, **6**, 285 (1963).
(21) P. A. Andrews, S. Mayburg, and J. A. Wall, *Sci. Tech. Aerosp. Rep.*, **4**, 1115 (1966).
(22) B. Mentro, J. Carmichael, and F. Karasz, 158th National Meeting of the American Chemical Society, New York, N.Y., 1969.
(23) S. D. Stookey, *Int. Glaskongr., [Fachvortr.], 5th*, 1 (1959).
(24) J. A. Koutsky, A. G. Walton, and E. Baer, *J. Appl. Phys.*, **38**, 1832 (1967).
(25) J. D. Hoffman and J. I. Lauritzen, Jr., *J. Res. Natl. Bur. Stand., Sect. A*, **65**, 297 (1961).
(26) J. N. Hay, M. Sabir, and R. L. T. Stevens, *Polymer*, **10**, 187 (1969).
(27) P. J. Flory and A. D. McIntyre, *J. Polym. Sci.*, **18**, 592 (1955).
(28) A. Rosenberg and W. C. Winegard, *Acta Metall.*, **2**, 242 (1954).
(29) J. B. Hudson, Thesis, Department of Chemistry, Rensselaer Polytechnic Institute, Troy, N.Y., 1958.
(30) K. Katayama, T. Amano, and K. Nakamura, *Kolloid Z. Z. Polym.*, **226**, 125 (1968).
(31) D. Hansen, A. N. Taskar, and O. Casale, *J. Polym. Sci., Part A-2*, **10**, 1615 (1972).
(32) P. A. Spegt, J. Terrisse, B. Gilg, and A. E. Skoulios, *Makromol. Chem.*, **107**, 29 (1967).
(33) H. Kim and L. Mandelkern, *J. Polym. Sci., Part A-2*, **6**, 695 (1968).
(34) L. Mandelkern, N. L. Jain, and H. Kim, *J. Polym. Sci., Part A-2*, **6**, 165 (1968).
(35) D. R. Beech and C. Booth, *J. Polym. Sci., Part B*, **8**, 731 (1970).
(36) A. M. Affifi-Effat and J. N. Hay, *J. Chem. Soc., Faraday Trans. 2*, **68**, 656 (1972).
(37) J. Q. G. Maclaine and C. Booth, *Polymer*, **16**, 191 (1975).
(38) J. L. Way, J. R. Atkinson, and J. Nutting, *J. Mater. Sci.*, **9**, 293 (1974).

Morphological Studies of Semicrystalline Poly(2,6-dimethylphenylene oxide)

W. Wenig, R. Hammel, W. J. MacKnight,* and F. E. Karasz

Polymer Science and Engineering, Chemistry Department, and Materials Research Laboratory, University of Massachusetts, Amherst, Massachusetts 01002. *Received September 8, 1975*

ABSTRACT: A sample of poly(2,6-dimethylphenylene oxide) (PPO) has been crystallized by exposure to 2-butanone (MEK) vapor. This sample has been investigated by wide and small angle x-ray scattering (WAXS and SAXS), differential scanning calorimetry (DSC), and light-scattering techniques. The WAXS and DSC experiments reveal a maximum crystallinity of about 30%. The SAXS, analyzed according to the linear paracrystal model of Hosemann, indicates a high degree of order in the superlattice with an average crystal lamellar thickness of 38 Å. Extensive peak broadening occurs in the WAXS curve arising from crystal lattice distortions or defects. These distortions or defects most probably are a consequence of the removal of solvent molecules from the lattice during the drying process. The light-scattering studies show a rodlike morphology apparently made up of fibrous bundles. The exact nature of the structures responsible for the observed light-scattering patterns cannot be conclusively demonstrated.

Wide angle x-ray-scattering (WAXS) studies of single crystals of poly(2,6-dimethyl-1,4-phenylene oxide) have been reported by a number of authors.[1–3] The results of the studies indicate that the structure of PPO single crystals depends on the solvent used for the crystallization and the subsequent drying procedures. Barrales-Rienda and Fatou[2] have shown that the relatively sharp diffraction maxima obtained in the WAXS pattern of PPO single crystals in the presence of α-pinene solvent become very broad and ill defined when the crystals are thoroughly dried. It is generally accepted that solvent molecules incorporate into the PPO crystal lattice.[2]

It is well known that bulk PPO cannot be thermally crystallized but crystallizes fairly readily in the presence of solvent or solvent vapor. Horikiri and Kodera[3] have reported the growth of spherulitic superstructures in PPO when thin films were exposed to α-pinene or tetralin. It was noted that spherulites are not formed when the crystallization is carried out in tetralin vapor at temperatures greater than 50 °C. This work demonstrates the dependence of the morphology as well as the crystal structure of PPO on the nature of the solvent and the conditions of crystallization. Solvents having solubility parameters close to that of PPO produce a morphology which is stable over a wide range of temperatures.[5,6] For the present study, 2-butanone (MEK) has been selected as the solvent. (MEK has a solubility parameter of 9.3 while PPO has a solubility parameter of 8.8.) In all cases the polymer films were thoroughly dried subsequent to crystallization. In the case of some solvents, such as acetone, the drying process leads to extensive crazing,[6] but no crazing was observable with MEK. The morphology and structure of the semicrystalline PPO thus obtained were studied by small angle x-ray scattering (SAXS), differential scanning calorimetry, (DSC), and light scattering, in addition to WAXS.

Experimental Section

(1) Sample Preparation. PPO was obtained from the General Electric Co. (courtesy of A. Katchman) in powder form. The powder was dissolved in toluene at 25 °C and precipitated with an excess of methanol. The PPO purified in this way was used for the crystallization experiments. $[\eta]$ was measured in toluene at 25 °C and interpreted with the aid of the viscometric equation of Barrales-Rienda[2]

$$[\eta] = 5.74 \times 10^{-2} \bar{M}_n^{0.69} \quad (1)$$

This resulted in an $\bar{M}_n$ of 2.3×10^4.

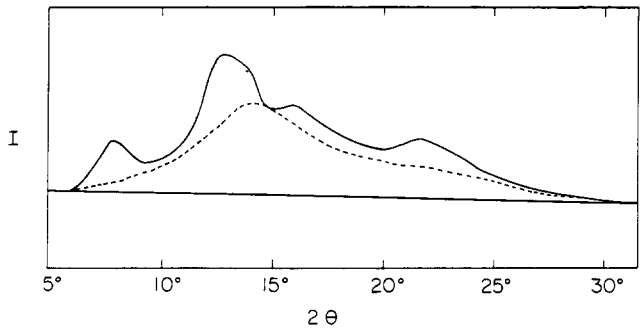

Figure 1. Wide-angle-x-ray scattering of a partially crystallized PPO sample as a function of the scattering angle 2θ. The WAXS curve of an amorphous standard has been constructed into the curve to separate the crystal peaks from the amorphous halo.

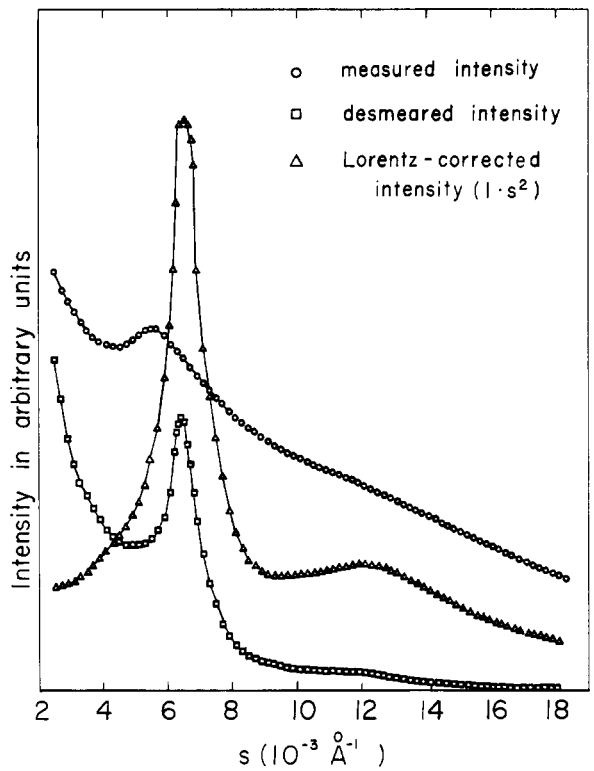

Figure 2. Small-angle-x-ray scattering curve of PPO. The registered intensity is displayed together with the slit-desmeared and Lorentz-corrected intensities. (The intensity scales of the curves are different.)

The dried PPO was compression molded into films of about 0.4 mm thickness at 10 000 psi and 280 °C under nitrogen. The molded films were cut to a final sample size of 25 × 15 mm.

Films were crystallized by exposure to an atmosphere of MEK vapor at 75 °C for 72 h. The crystallized films were then dried under vacuum at 110 °C for 24 h. After this treatment no residual solvent could be detected.

(2) Measurements. (a) WAXS. WAXS measurements were carried out with a Philips-Norelco wide angle goniometer equipped with a graphite monochromator. The goniometer was used in the symmetrical reflection mode in order to obtain good resolution of the crystalline diffraction peaks. The intensity was corrected for absorption and a correction was made for instrumental broadening using a silicon standard provided by Philips. The integral breadths of four peaks were measured by planimetry, plotted against Bragg angle (2θ), and extrapolated to smaller angles.

WAXS curves were also obtained from completely amorphous samples in order to effect a separation of the amorphous and crystalline scattering.

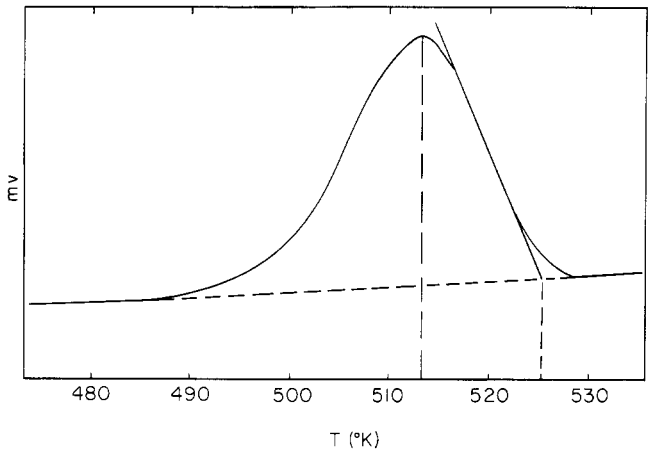

Figure 3. DSC thermogram of PPO.

The areas under the WAXS curves for both the amorphous and crystalline samples were measured by planimetry in the range 2θ = 7° to 2θ = 30°. This range encompasses all the crystalline diffraction peaks with the exception of a few weak peaks of higher order. These are difficult to separate from the background and make only a small contribution to the overall scattering intensity.

The WAXS patterns of both amorphous and crystalline PPO are shown in Figure 1.

Photographic flat plate patterns demonstrate that no preferred orientation direction exists in any of the samples.

(b) SAXS. SAXS investigations were carried out with a Rigaku-Denki small-angle camera equipped with a Kratky collimation system.[7] Cu Kα radiation was used and monochromatization was achieved with a Ni filter in conjunction with electronic pulse height analysis of the output from a proportional counter. The x-ray generator was housed in a constant-temperature room and the temperature of the cooling water for the x-ray tube was controlled to provide a constant primary beam intensity.

Both scattering curves and background intensity were recorded with a minimum of 5000 counts per point in order to minimize experimental error. Since the Kratky collimation system operates with slits, the experimental scattering curves are "slit smeared". Desmearing of the experimental curves was accomplished by the method of Schmidt[8] and that of Guinier and Fournet.[9,10] Both methods gave essentially the same results.

Lorentz corrected SAXS curves were obtained by multiplying the intensities of the desmeared curves by s^2 ($s = 2 \sin \theta/\lambda$). Figure 2 shows the experimental curve, the desmeared curve, and the Lorentz corrected curve for a sample of crystalline PPO.

(c) DSC. Melting points and heats of fusion were measured using a Perkin-Elmer calorimeter Model DSC-2. Calibration was achieved with an Indium standard. A typical thermogram of a crystalline PPO sample is shown in Figure 3. The heating rate in this case was 10 °C/min.

(d) Light Scattering. Light-scattering patterns were obtained from the crystalline PPO samples using an apparatus designed by Stein.[11] A laser source was used in conjunction with a polarizer to ensure complete linear polarization. After the polarized light beam passed through the sample a second polarizer was used whose polarization axis was either perpendicular to that of the first polarizer (H_v pattern) or parallel to that of the first polarizer (V_v pattern). Samples having thicknesses of <0.005 cm were pressed between glass plates in the presence of an immersion liquid (silicon oil) having approximately the same refractive index as the sample.

Results and Discussion

(1) Crystallinity. An inspection of Figure 1 reveals that the crystalline diffraction peaks in PPO are quite broad and ill defined. The scattering pattern is quite similar to that obtained by Barrales-Rienda and Fatou[2] for dried single-crystal mats of PPO. It is probable that the removal of the solvent introduces lattice defects which result in a very imperfect crystal structure.

An approximate value of the weight fraction of crystalline material may be obtained using:

Table I
Crystallinities W_c of PPO Obtained from Various Experimental Methods

Method	W_c, %
WAXS	31
SAXS	25[a]
DSC	33

[a] Linear crystallinity ϕ_C obtained by theoretical model calculations of SAXS curves.

$$W_c = \frac{\int_0^\infty I_c(s)s^2\,ds}{\int_0^\infty I(s)s^2\,ds} = \frac{\int_0^\infty I(s)s^2\,ds - \int_0^\infty I_a(s)s^2\,ds}{\int_0^\infty I(s)s^2\,ds} \quad (2)$$

W_c = weight fraction crystallinity; $I_c(s)$ = crystalline scattering intensity at s; $s = 2\sin\theta/\lambda$, where θ is half the scattering angle and λ is the wavelength of the x-ray source; $I(s)$ = total scattering intensity at s; $I_a(s)$ = amorphous scattering intensity at s.

In order to obtain meaningful values from this method, the amorphous halo must be resolvable from the scattering due to crystalline material. Such a resolution is very difficult in the case of crystalline PPO due to the broadness of the crystalline peaks. In order to overcome this difficulty, the scattering curve of amorphous PPO (Figure 1) was subtracted from that of crystalline PPO.[12] The value for W_c obtained by this method is listed in Table I.

For a partially crystalline material which contains crystals of "infinite" dimensions, the weight fraction crystallinity may be obtained from the relationship

$$W_c = \Delta Q_f/\Delta H_f \quad (3)$$

ΔQ_f = observed enthalpy of fusion; ΔH_f = enthalpy of fusion of a completely crystalline material. ΔQ_f is proportional to the area under the DSC melting endotherm and ΔH_f has been determined previously for PPO using the "diluent" technique.[13] Values obtained from eq 3 can be in error when the crystals are small. We may write

$$\Delta H_f = \Delta H_{f\infty} - (2\sigma_e/l) \quad (4)$$

ΔH_f = enthalpy of fusion for crystals of thickness l; σ_e = surface free energy of the crystals.

Although values for l have been obtained for crystalline PPO by SAXS as will be discussed subsequently, no values for σ_e are available. It is thus impossible to quantitatively assess the error introduced into W_c using eq 3. The value of W_c obtained from eq 3 would be expected to be an underestimate. Table I reveals that this value agrees quite well with that obtained from WAXS. (The WAXS result would also be expected to be an underestimate since WAXS is insensitive to small crystals.)

The Lorentz corrected SAXS curve shown in Figure 2 exhibits two maxima. The more prominent of the two maxima occurring at the lower angle corresponds to a Bragg spacing of 160 Å. This will be referred to as the long period L^+. The second maximum is presumed to be a second order of the long period maximum although its angular position is somewhat less than double that of the long period maximum. The overall shape of the Lorentz corrected SAXS curve is very reminiscent of that of many other semicrystalline polymers which have highly ordered superstructures.

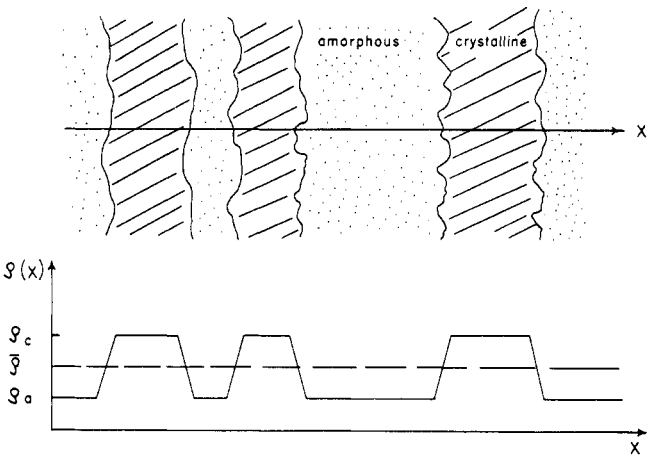

Figure 4. Model of the crystalline superstructure of PPO ("sandwich model"). The electron density $\delta(x)$ is assumed to drop linearly from g_c to g_a due to thickness variations of the crystalline layers.

In order to interpret the SAXS curve to obtain parameters pertaining to the superstructure of crystalline PPO it is necessary to assume a model and fit the experimental results to this model. The model assumed is a one-dimensional model[14] in which the lamellar crystals in the system are arranged in domains of limited size. It is required that every crystalline lamella be followed by an amorphous layer, the succeeding crystal lamella being orientation correlated to the preceding. The number, N, of crystals in a domain is allowed to vary. Thus the domains are polydisperse in size and the modulation of the SAXS curve is due to electron density fluctuations within a domain. Hence the theoretical intensity function, $I(s)$, for the model, can be calculated from the inner structure of an average domain. A strict two-phase system is assumed (one crystalline density and one amorphous density) and the average scattering intensity $\bar{I}(s)$ calculated from Hosemann's equations for a linear paracrystalline lattice.[15]

$$\begin{aligned} \bar{I}(s) &= I_A + I_B \\ I_A &= \frac{1}{2\pi^2 s^2} R_e\left\{N\left[\frac{(1-f_x)(1-f_y)}{1-f_z}\right]\right\} \\ I_B &= \frac{1}{2\pi^2 s^2} R_e\left\{f_y\left(\frac{1-f_x}{1-f_z}\right)^2(1-f_z^N)\right\} \\ f_x &= \int_{-\infty}^{\infty} h(x_c)\exp(-2\pi i s x_c)\,dx_c \\ f_y &= \int_{-\infty}^{\infty} h(x_a)\exp(-2\pi i s x_a)\,dx_a \\ f_z &= f_x \cdot f_y \end{aligned} \quad (5)$$

$h(x_c)$ = thickness distribution function of the crystalline phase; $h(x_a)$ = thickness distribution function of the amorphous phase; x_c = thickness of a particular crystalline lamella; x_a = thickness of a particular amorphous layer.

Equation 5 presumes the existence of an infinitely sharp boundary between the crystalline phase and the amorphous phase, which is somewhat unrealistic. In order to account for a diffuse boundary layer, an interfacial region is assumed in which the density changes linearly from the crystalline to the amorphous density as illustrated in Figure 4. The contribution of this interfacial region to the SAXS scattering curve has been discussed by Tsvankin[16] and leads to a modification of eq 5 as

Table II
Superstructure Parameters Obtained by Fitting Theoretical SAXS Curves to the Experimental Curve[a]

Distribution function combination $(hx_c)/(h(x_a)$	$\bar{x}_c$, Å	$\bar{x}_a$, Å	$\bar{x}_b$, Å	g_c, %	g_a, %	W_c, %	N	δ, %
Symm/symm	38	114	10	30	25	25	14	1.96
							∞	5.98
Symm/unsymm[b]	45	104	10	33	30	30	14	44.1
Unsymm/unsymm	31	116	10	45	20	21	18	48.3

[a] The parameters listed are those of the closest fit. [b] Equivalent to the combination unsymm/symm.

$$\bar{I}(s) = [I_A + I_B]z(s)$$

$$z(s) = \frac{1}{(2\pi \text{ is } \bar{x}_b)^2}|1 - \exp(-2\pi \text{ is } \bar{x}_b)|^2 \tag{6}$$

$\bar{x}_b$ = average thickness of the interfacial layer.

In the case of large numbers of orientation correlated crystals, the contribution of I_B to $\bar{I}(s)$ becomes negligible and eq 6 reduces to

$$\lim_{N\to\infty} \bar{I}(s) = I_A \cdot z(s) \tag{7}$$

In order to obtain the proper distribution functions $h(x_c)$ and $h(x_a)$ to fit the experimental curve, different combinations of symmetrical and unsymmetrical functions were tried.[17] Initially N was assumed large and the distribution functions obtained using eq 7. After the distribution functions had been determined, N was allowed to vary and eq 6 was used for the final "best" fit.

The forms of the trial distribution functions were

$$h(x_i) = \frac{1}{\bar{x}} \exp\left(-\frac{x_i}{\bar{x}_i}\right) \tag{8}$$

for the unsymmetrical distribution functions and

$$h(x_i) = \left[\frac{1}{(2\pi\Delta^2\bar{x}_i)^{1/2}}\right] \exp\left[-\frac{(x_i - \bar{x}_i)^2}{2\Delta^2\bar{x}_i}\right] \tag{9}$$

for the symmetrical distribution functions.

In eq 8 and 9 x_i refers to either the crystalline or amorphous thickness and $\Delta^2\bar{x}_i$ refers to the mean-square fluctuation in thickness of either the crystalline or amorphous phase. The results of the calculations are collected in Table II. The thickness fluctuations are designated g_c and g_a in Table II and are related to the $\Delta^2\bar{x}_i$ by

$$g_c = \Delta^2\bar{x}_c/\bar{x}_c^2$$
$$g_a = \Delta^2\bar{x}_c/\bar{x}_a^2 \tag{10}$$

The fluctuations g_c and g_a following from eq 8 have been determined graphically.[17] The deviation of the theoretical from the experimental curve, δ, is given by

$$\delta^2 = (s_{max} - s_{min}) \frac{\int_{s_{min}}^{s_{max}} (I_{th}(s) - I_{exptl}(s))^2 \, ds}{\left(\int_{s_{min}}^{s_{max}} I_{exptl(s)} \, ds\right)^2} \tag{11}$$

An inspection of the δ's in Table II reveals that only the combination of symmetrical $h(x_i)$'s for both the amorphous and crystalline phases yielded a close fit to the experimental data. The best fit with $h(x_i)$ of the form of eq 9 is shown in Figure 5a while Figure 5b shows the best fits obtainable with the other combinations of $h(x_i)$'s. The $h(x_i)$'s which gave the best fit are shown in Figure 6.

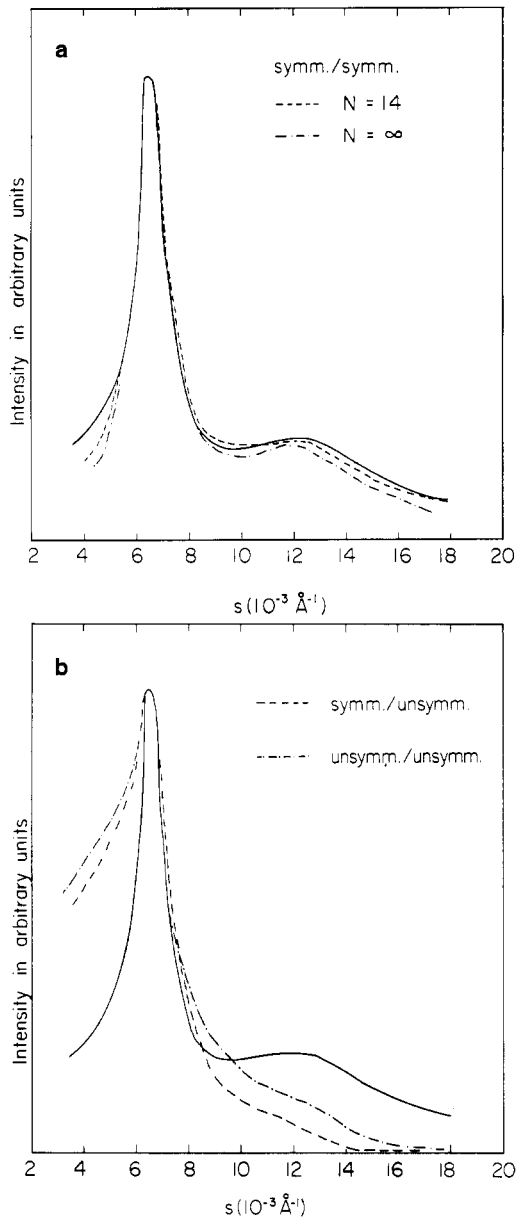

Figure 5. (a) Experimental and calculated SAXS functions using symmetrical functions for both crystal and amorphous thickness distributions. Calculated curves are shown for N = 14 giving the closest fit and for N = ∞ which still shows a good match. (b) Experimental and calculated SAXS functions using thickness distributions other than symmetrical.

The parameter N is relatively insensitive to variations. The best fit was obtained with N = 14, but calculated curves with $N > 14$ do not deviate from the experimental results by more than 6%, which is about the experimental error. There is, however, a very strong increase in δ for values of $N < 14$. It is thus clear that there is a high degree of order within a domain, even allowing for the approximate character of the model.

As is also shown in Table II, $\bar{x}_c$ is found to be 38 Å. The lamellae are thus very thin. Contrasted with this is the value of $\bar{x}_a$ of 114 Å. The low value of $\bar{x}_c$ is consistent with the anomalously high value of (T_g/T_m) in PPO, about 0.9.[13] The reason why the lamellae do not grow thicker is unknown at present.

Figure 7 shows the H_v light-scattering pattern from a crystalline PPO film. The pattern is not spherulitic in nature but is consistent with a superstructure of unoriented,

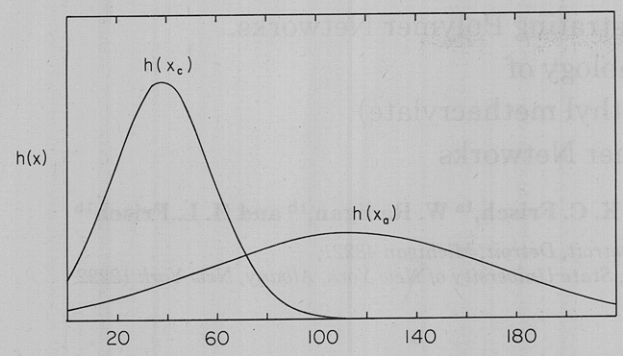

Figure 6. Thickness distribution functions calculated with the parameters of the closest SAXS fit.

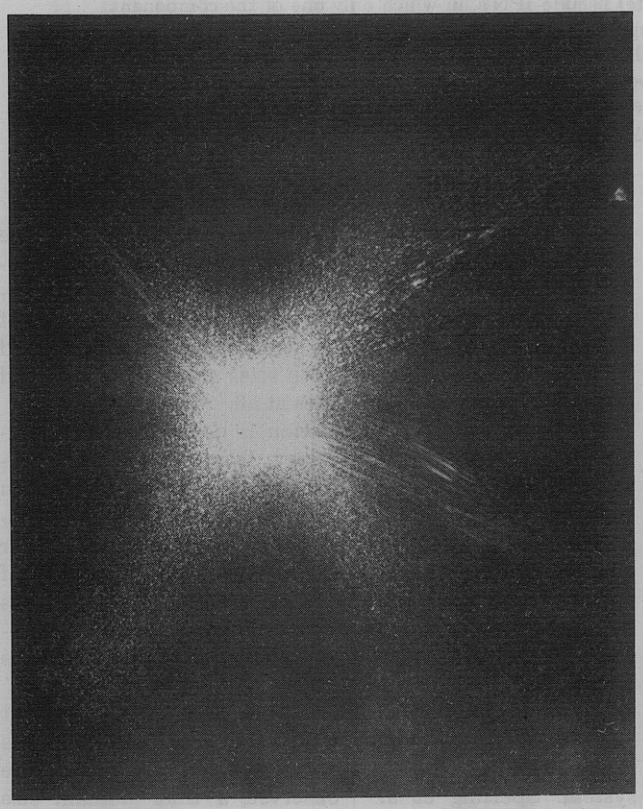

Figure 7. H_v light-scattering pattern of PPO.

rodlike entities.[18] If the rods were to consist of clusters of randomly oriented fibrous bundles, this would explain the relatively high degree of order revealed by the SAXS measurements. It is well known that many polymers can be crystallized to yield the so called "shish-kebab" morphology in which chain-folded crystal lamellae are stacked on a central core. This morphology has only been obtained, however, in the presence of a strong shear field or other orienting mechanism. It is to be doubted, although some shear flow exists during the compression molding of the films, that sufficient orientation can exist in the PPO samples to lead to the development of "shish-kebab" morphologies.

Conclusions

(1) Bulk PPO can be crystallized by exposure to MEK vapor to the extent of about 30%.

(2) The crystal lattice is strongly distorted, probably due to the presence of defects introduced by the removal of solvent molecules from the lattice during the drying process.

(3) The crystal lamellae are arranged in a superlattice with a high degree of order.

(4) The crystal lamellae are very thin, consistent with the high (T_g/T_m) ratio in PPO.

(5) The thickness distribution functions of both the crystal and amorphous layers are best represented by symmetrical distribution functions.

(6) The superstructure is not spherulitic in nature, but appears to consist of rodlike entities composed of clusters of fibrous bundles.

Acknowledgment. This work was supported by Materials Research Laboratory Grant GH 38347 and, in part, by AFOSR 72-2170 (F.E.K).

References and Notes

(1) C. C. Price, W. A. Butte, and R. E. Hughes, *J. Polym. Sci.*, **61**, 28 (1962).
(2) J. M. Barrales-Rienda and J. M. G. Fatou, *Kolloid Z. Z. Polym.*, **244**, 317 (1971).
(3) S. Horikiri and K. Kodera, *Polym. J.*, **4**, 213 (1973).
(4) A. G. Shwarts, *Kolloid. Zh.*, **18**, 753 (1956).
(5) R. Neira-Lemos, Ph.D. Thesis, University of Massachusetts, Amherst, Mass., 1974.
(6) R. Neira, F. E. Karasz, and W. J. MacKnight, in preparation.
(7) O. Kratky, *Z. Elektrochem.*, **62**, 66 (1958).
(8) P. W. Schmidt, *Acta Crystallogr.*, **19**, 938 (1965).
(9) A. Guinier and G. Fournet, *J. Phys. Radiation*, **8**, 345 (1947).
(10) O. Kratky, G. Porod, and Z. Skala, *Acta Phys. Austriaca*, **13**, 76 (1960).
(11) R. S. Stein, "Newer Methods of Polymer Characterization", Wiley, New York, N.Y., 1964, Chapter IV.
(12) L. E. Alexander, "X-Ray Diffraction in Polymer Science", Wiley, New York, N.Y., 1969.
(13) F. E. Karasz, H. E. Bair, and J. M. O'Reilly, *J. Polym. Sci., Part A-2*, **6**, 1141 (1968).
(14) W. Wenig, F. E. Karasz, and W. J. MacKnight, *J. Appl. Phys.*, **46**, 4194 (1975).
(15) R. Hosemann and S. M. Baghchi, "Direct Analysis of Diffraction by Matter", North-Holland Publishing Co., Amsterdam, 1965.
(16) D. Ya. Tsvankin, *Polym. Sci., USSR* (*Engl. Transl.*), **6**, 2304 (1964).
(17) R. Brämer, *Colloid Polym. Sci.*, **252**, 504 (1974).
(18) M. B. Rhodes and R. S. Stein, *J. Polym. Sci., Part A-2*, **7**, 1539 (1969).